INTL JOURNAL OF ELECTRONICS AND TELECOMMUNICATIONS, 2026, VOL. 72, NO. 2, PP. 1-9
Manuscript received January 22, 2026; revised April, 2026. doi: 10.24425/ijet.2026.157902

Compact broadband Circularly Polarized Truncated Parasitic Patch Antenna

J Nageswara Rao, and R Ramana Reddy

***Abstract*—In this paper design of a microstrip patch antenna, incorporating parasitic patches and Defective Ground Structure (DGS) to achieve wide bandwidth, high gain and circular polarization is presented. The initial single-patch design operating at 5.55 GHz showed poor impedance matching (-4.52 dB), limited bandwidth, and no circular polarization. To overcome these issues, parasitic patches were added, resulting in dual-band operation at 5.25 GHz and 7.45 GHz, with enhanced return losses of -14.64 dB and -12.04 dB, with impedance bandwidths of 190 MHz and 160 MHz, respectively. The 100 MHz axial-ratio bandwidth was the first step towards achieving circular polarization. Further optimization resulted in a wideband resonance at 6.1 GHz, with a bandwidth of 1.12 GHz (5.12–6.24 GHz) and an improved axial-ratio bandwidth of 1.10 GHz (5.09–6.20 GHz). The gain increased to 10.7 dBi. In the final phase incorporation of H-shaped DGS resulted in a broadband of 2.12 GHz (4.07–6.19 GHz) and axial-ratio bandwidths of 360 MHz and 870 MHz. The recommended antenna is appropriate for satellite communications and radar applications.**

***Keywords*—Parasitic Patch; Circular Polarization; High Gain; DGS**

I. INTRODUCTION

IN modern wireless communication systems, CP antennas are crucial to help improve polarization mismatches, mitigate multipath fading, and ultimately improve signal reliability. This makes CP antennas particularly attractive for applications such as satellite communications, global positioning systems, and radio-frequency identification. Among these different designs of CP antennas, microstrip patch antennas remain desirable due to their low-profile and lightweight characteristics and ease of integration. However, conventional single-feed patch antennas commonly suffer from narrow bandwidths below 10% for impedance and axial ratio.

Different methods have been investigated to improve the axial ratio (AR) bandwidth of circularly polarized antennas. In [1], a low-profile broadband CP antenna featuring an integrated dual-feeding network is described, where a directly fed CP patch combined with several parasitic patches greatly enhances both the matching and AR bandwidth, resulting in a matching bandwidth of 38% and a 3-dB axial-ratio bandwidth of 28.1%. Reference [2] reports a compact stacked patch antenna with a single-feed mechanism for wide bandwidth CP operation. The antenna is realized by integrating a truncated main patch, parasitic patches, and coaxial feeding, thus providing a 3-dB axial-ratio bandwidth of 20.7% and gain greater than 7.9 dBi. To improve gain and bandwidth while keeping the design simple, a single-layer CP antenna with a squared patch and symmetrical parasitic elements is introduced in [3], achieving an axial-ratio bandwidth of 14.7% and a gain of 9.1–10.8 dBi. A novel approach employing crossed dipoles and vertical plate structures is introduced in [4], aiming to enhance both bandwidth and beam width, resulting in a matching bandwidth of 92.6% and a 3-dB AR bandwidth of 71.8%. A different strategy is used in [5], where a perturbed ring resonator is incorporated into a CP patch antenna, producing a stable high gain of approximately 11 dBi over a 6% axial-ratio bandwidth while maintaining a compact design factor.

Several studies have investigated alternative feeding structures and ground modifications to optimize CP antenna performance. An aperture-stacked patch (ASP) antenna with four parasitic patches is reported in [6], achieving a 3-dB AR bandwidth of 33.6% for a single element and 36.15% in an array configuration, highlighting its wideband characteristics. Additionally, explored how DGS can improve impedance matching and AR bandwidth while maintaining a low-profile design [7]. A CP antenna that combines elements of different shapes to enhance performance is proposed in [8], achieving an axial-ratio bandwidth of 11% and a gain exceeding 9.1 dBi, making it an appropriate candidate for satellite communication applications.

Parasitic elements and resonators have also been used for broadband CP performance. A parasitic loop-loaded crossed dipole antenna is presented in [9]. It has a 3-dB axialratio bandwidth of 28.6% with a high gain of 8.34 dBi. The work has also explored 1×2 and 2×2 array configurations for further enhancing performance. A sequential-phase feeding network in the CP patch array is used in [10]. The proposed design has attained an AR bandwidth of 12.7% with a high gain of approximately 12 dBi. By incorporating multiple CP operating modes, this work presents an effective method to further improve the AR bandwidth beyond that achievable by a conventional single-layer design. Various works have been done to improve the AR bandwidth of CP antennas. A broadband CP antenna array integrated with a sequential-phase feeding network along with parasitic elements is proposed in [11]. It has an axial-ratio bandwidth of 11.8% with a high gain of 12.5 dBi. Similarly, a stacked patch antenna configuration was studied in [12] with two parasitic elements,

First Author is with Research Scholar, Department of ECE, JNT University Anantapur, Andhra Pradesh, and Department of ECE, JNTUA College of Engineering, Pulivendula, Andhra Pradesh, India (e-mail: jadanageswararao@gmail.com).

Second Author is with Department of ECE, JNTUA College of Engineering, Kalikiri, Andhra Pradesh, India (e-mail: profrrreddy@yahoo.co.in).

one for bandwidth enhancement and the other for improving gain. It yielded an impedance bandwidth of more than 12%. These results demonstrate the effectiveness of parasitic structures in broadband and high-gain performance.

Another widely studied method involves using defected ground structures (DGS) to improve antenna features. How DGS can be applied to microstrip antennas to shift the resonance frequency, reduce mutual coupling, and increase bandwidth, making it an effective approach for compact CP antenna designs, was discussed in [13]. The incorporation of DGS with a miniature microstrip patch antenna is examined in [14], demonstrating a resonance frequency shift from 10 GHz to 3.5 GHz, confirming its potential for size decrease without sacrificing performance. Stacked patch antennas have also been extensively studied for broadband CP operation. A stacked patch design is presented [15] for GPS applications, using three stacked elements with slits and I-slot structures to achieve triple-band operation. Similarly, a stacked patch antenna with a single feed is projected in [16], optimized for wideband circular polarization, maintaining stable AR performance across multiple frequency bands. These studies show that stacking techniques effectively overcome the limitations of conventional single-layer CP antennas.

Alternative feeding mechanisms have been explored to improve CP bandwidth and gain. Novel crossed-dipole design using near-field resonant parasitic (NFRP) elements is presented in [17] to achieve dual-band and broadband CP performance. This technique thus enables the design of compact high-efficiency CP antennas for multi-frequency applications. Furthermore, a coupled, rotated, vertical metallic plate structure is proposed in [18] in order to enrich the bandwidth of CP crossed-dipole antennas, which achieves over 106% increase. DRAs have also been investigated for broadband CP applications: A circularly polarized DRA excited by an external tape helix is discussed in [19], exhibiting a 3-dB Axial-Ratio bandwidth of 6.4%. A stacked dielectric resonator antenna configuration optimized for wideband CP operation [20] underlines the role of dielectric material in enhancing bandwidth.

The use of probe-fed stacked patches has been widely explored to improve matching bandwidth and radiation efficiency. A design strategy for probe-fed stacked patches was discussed in [21], achieving bandwidths exceeding 25% by optimizing dielectric substrate selection and impedance control techniques. This work highlights that impedance matching is the key to achieving broadband performance in stacked patches. Further, a sequentially phase-fed CP antenna array with a slotted metal wall is also proposed in [22], which achieves a matching bandwidth of 20.8% and a 3-dB AR bandwidth of 17.6%, proving that sequential-phase feeding offers a good method to achieve a wide bandwidth and high gain. The design for the parasitic element-based CP antenna has also been one of the intensive research aspects. A wideband CP patch antenna with parasitic strips was proposed in [23] to achieve a 3-dB AR bandwidth of 24% with an appropriate arrangement of sequentially rotated strips surrounding the main patch. Again, this work shows that capacitive coupled feeding structure and parasitic elements are quite necessary for wideband CP operation. Likewise, a CP array antenna that makes use of a sub-grid array with linearly polarized elements was also proposed in [24] for highly integrated radio applications at 60 GHz, while sequentially rotated sub-arrays and optimized feeding network enabled wide impedance bandwidth and AR bandwidth.

The study demonstrates several challenges in designing CP DRAs, including achieving a widespread axial-ratio bandwidth and optimizing the feed mechanisms [25]. Ensuring stable circular polarization across a wide frequency range remains a key concern, requiring innovative design solutions and advanced simulation techniques. The work demonstrates that curved slot designs significantly enhance CP performance compared to traditional rectangular slot approaches [26]. The use of curved slots improves the axial-ratio bandwidth, ensuring more reliable CP radiation across a wider frequency range. The performance improvements make these antennas suitable for a variety of wireless communication applications.

Next, the document is prearranged as follows: Section 2 describes the future antenna design in four phases as detailed in the text. Following that, Section 3 presents the results and discussion of the performance. The final section provides the conclusion of the study.

II. PROPOSED DESIGN

The proposed antenna design was developed through a systematic evolution process, incorporating various structural modifications to improve its impedance bandwidth, gain, and axial-ratio bandwidth, thereby achieving stable circular polarization. Fig. 1 shows the front view of the proposed circularly polarized patch antenna. The design iterations included introducing parasitic patches, implementing bandwidth enhancement techniques, and implementing a DGS to achieve a wider operational range. Table 1 shows the physical dimensions of the proposed antenna, including substrate size, patch widths, and spacing. These dimensions guide the design implementation in simulation and fabrication.

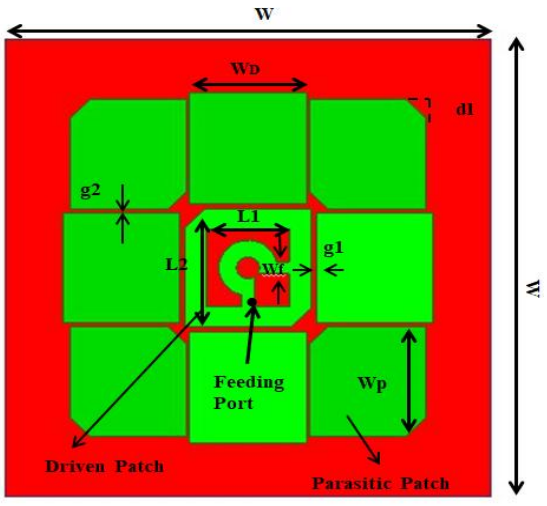

Fig. 1 Proposed antenna (front view)

TABLE I
DIMENSIONS OF ANTENNA

Dimension	Value (mm)
Width of substrate (W)	50
Width of parasitic patch (W_D)	12
Length of parasitic patch (W_P)	12
Width of feed (W_F)	1.3
Radius of inner circle (R1)	3
Radius of outer circle (R2)	1.2
Dimension of inner square (L1)	8.5
Dimension of outer square (L2)	12.9
Dimension of Truncated curve (dl)	2
Gap between patch and driven patch (g1)	0.6
Gap between parasitic and driven patch (g2)	0.35

PROPOSED ANTENNA EVOLUTION:

CONVENTIONAL RECTANGULAR PATCH ANTENNA

An MPA consists of radiating patches supported by a ground plane. A traditional RPA with dimensions of 26 x 28 mm is created for 10 GHz on the Roger RT-Duroid 5880 substrate. The substrate has a dielectric constant (εr) of 2.2, and its dielectric loss tangent (δ) is 0.0009 mm. Figure 1 shows the schematic diagram for a proposed patch antenna. Applying Equations (1) and (2), the patch's width (W) and length (L) can be determined [3].

$$w = \frac{c}{2fr}\sqrt{\frac{2}{\epsilon r+1}} \quad \text{---------- (1)}$$

$$L = \frac{e}{2fr\sqrt{\epsilon eff}} - 2\Delta L \text{---------- (2)}$$

Where, εreff is the Effective dielectric constant, W is the width of the rectangular patch, εr is the dielectric constant, and c is the speed of light.

A standard rectangular microstrip patch antenna is first designed using standard equations (1) and (2) for length and width, based on substrate and target frequency. Bandwidth is improved and circular polarization is obtained by introducing edge truncation and inner rectangular slots. Next, a C-shaped circular slot etched within the patch further broadens the impedance bandwidth and enables multi-band resonance, making the antenna suitable for advanced wireless systems**.**

This section presents the proposed antenna design, which is developed in four phases to achieve the desired multiband and wideband performance.

Phase 1: Initial Single Patch Configuration

In the first phase, the antenna was designed as a simple microstrip patch operating at 5.55 GHz, as illustrated in Fig. 2. However, this initial design exhibited poor impedance matching, with a return loss (RL) of only -4.52 dB, indicating significant signal reflection. Furthermore, the bandwidth was 0 MHz, meaning the antenna could not operate efficiently over a range of frequencies. The gain was 6.8 dBi, but the antenna failed to attain circular polarization, as no axial-ratio bandwidth was observed. This limited performance highlighted the need for structural modifications to increase impedance matching, bandwidth, and polarization characteristics.

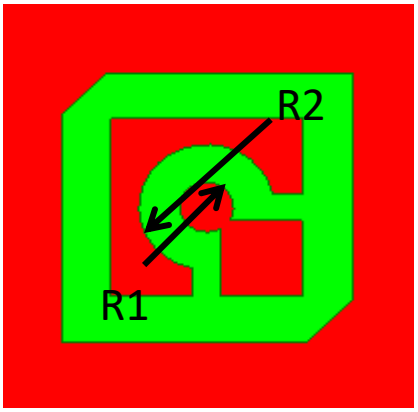

Fig. 2. Simple microstrip patch antenna

Phase 2: Introduction of Parasitic Patches for Dual-Band Operation

To improve impedance matching and enrich the antenna's bandwidth, parasitic patches were introduced around the driven patch, as demonstrated in Fig.3. These patches electromagnetically coupled with the main radiator, resulting in dual-band resonance at 5.25 GHz and 7.45 GHz. The reflection loss significantly improved to -14.64 dB and -12.04 dB, respectively. The antenna now exhibited increased impedance bandwidths of 190 MHz (5.19–5.38 GHz) and 160 MHz (7.37–7.53 GHz). The gain also increased to 8 dBi at 5.25 GHz and 11.2 dBi at 7.45 GHz, indicating better radiation efficiency. Circular polarization began to develop, with an axial-ratio bandwidth of 100 MHz (6.98–7.08 GHz), marking an important step towards achieving stable CP operation. However, further refinements are needed to broaden the axial-ratio bandwidth and improve the CP characteristics.

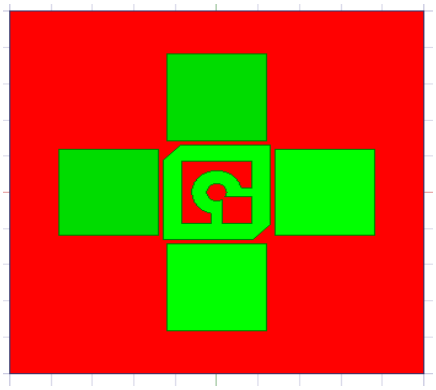

Fig. 3 Parasitic Patch antenna

Phase 3: Optimisation for Wideband Performance

In this phase, additional modifications were made to optimise the dimensions of the driven patch and parasitic patches, as illustrated in Fig. 4, while adjusting their spacing to improve bandwidth and impedance matching. These refinements resulted in a single wideband resonance at 6.1 GHz, with a highly optimised return loss of -29.10 dB. The

impedance bandwidth increased to 1.12 GHz (5.12–6.24 GHz), enabling more efficient operation over a wider frequency range. Additionally, the gain was improved to 10.7 dBi, making the antenna highly suitable for high-gain applications.

The AR bandwidth expanded to 1.10 GHz (5.09–6.20 GHz), further stabilizing circular polarization performance. This phase achieved significant improvements in bandwidth and polarization characteristics, though additional changes were required for multi-resonant behavior. Fig. 5 shows the S-parameters, axial ratio, gain, and directivity for Phases 1–3, illustrating progressive enhancements in return loss and bandwidth at each stage. Fig. 6 presents the axial-ratio plots for Phases 1, 2, and 3. At 6 GHz, the antenna achieves an AR value of 1.2 dB, indicating excellent circular polarization performance and minimal polarization distortion. The structural evolution led to an extended AR bandwidth of up to 1.11 GHz and improved circular polarization. Fig. 7 presents the gain plots for Phases 1, 2, and 3, demonstrating a gain enhancement from 6.8 dBi to 10.7 dBi. Fig.8 shows the directivity plots across the three design phases, revealing improved directional radiation performance. The antenna patterns (E-Plane and H-Plane) for Phase 3 display a focused directional lobe, indicating a higher gain (around 10.7 dBi), as shown in Fig. 9. The symmetry also supports good circular polarization.

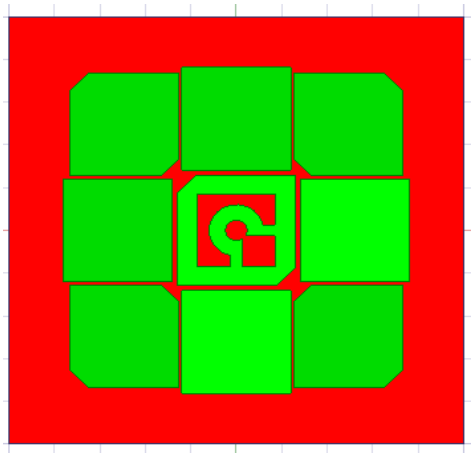

Fig. 4. Parasitic Patch antenna with driven patches

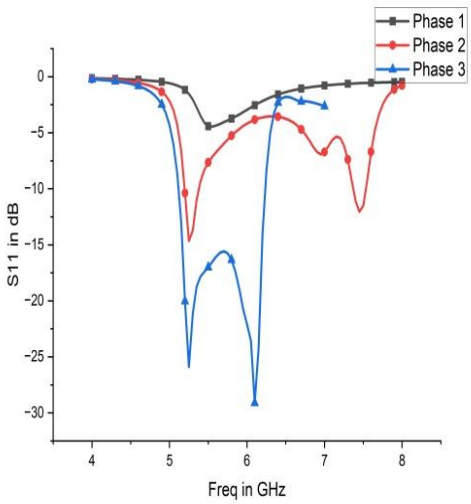

Fig. 5. S-Parameter plots of Phase 1, 2 and 3 antennas

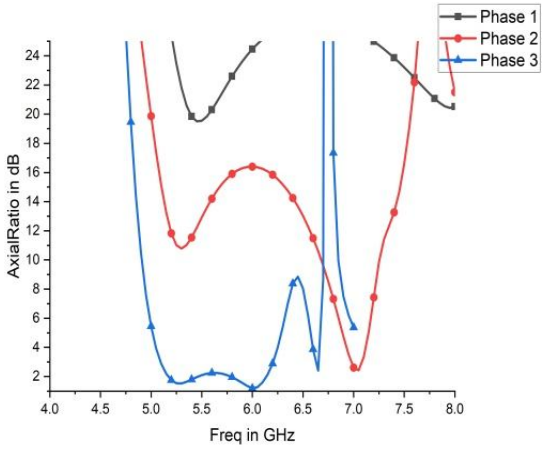

Fig. 6. Axial Ratio plots of Phase 1, 2 and 3 antennas

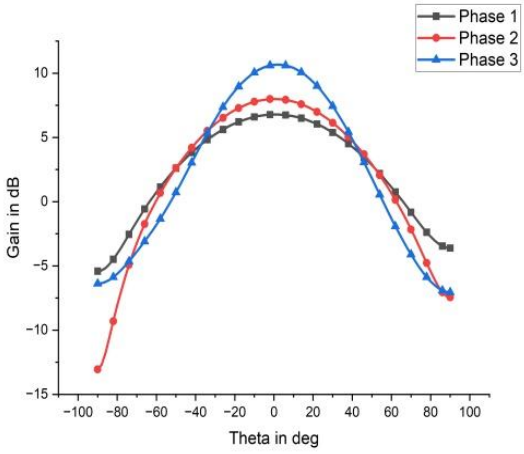

Fig. 7. Gain plots of Phase 1, 2 and 3 antennas

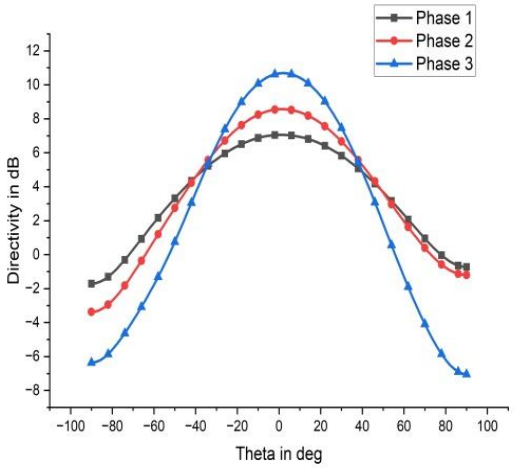

Fig.8. Directivity Plots of Phase 1, 2 and 3 antennas

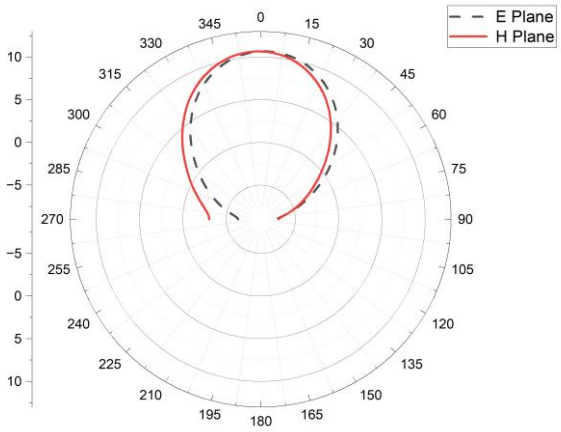

Fig. 9. Radiation pattern plot of Phase 3 antenna

Phase 4: Introduction of a DGS for Ultra-Wideband Performance

To further progress the antenna's bandwidth and polarization characteristics, an H-shaped DGS was introduced, as shown in Fig. 10. The DGS altered the current distribution on the ground plane, enhancing impedance matching and extending the bandwidth. With this modification, the antenna resonated at 4.95 GHz, with an exceptionally low reflection loss of -35.85 dB, indicating excellent impedance matching. The impedance bandwidth was further increased to 2.12 GHz (4.07–6.19 GHz), making the antenna highly appropriate for ultra-wideband (UWB) applications. However, a slight reduction in gain to 6.5 dBi was observed, a trade-off for achieving a broader bandwidth. Circular polarization was significantly improved, with axial ratio bandwidths of 360 MHz (4.58–4.94 GHz) and 870 MHz (5.33–6.20 GHz), ensuring consistent CP performance across multiple frequency bands. Fig. 11 presents the S-parameter plots for Phases 3 and 4, highlighting that the DGS further improved the return loss and bandwidth.

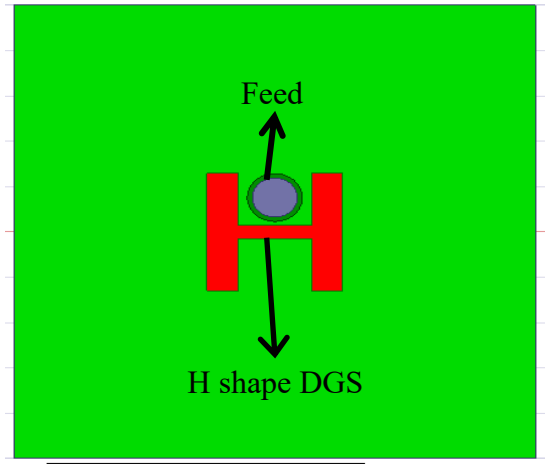

Fig. 10. Proposed antenna with inclusion of DGS

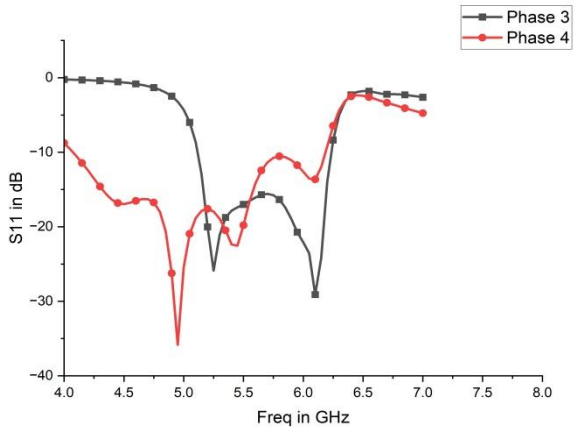

Fig. 11. S-Parameter plots of Phase 3 and 4 antennas

Fig. 12 illustrates the directivity plots comparing the Phase 3 and Phase 4 antennas. Fig. 13 shows axial-ratio plots after incorporating DGS, confirming an enhanced AR bandwidth and a consistent CP. At 4.8 GHz & 5.65 GHz, the antenna achieves an AR value of 1.1 & 1 dB, indicating excellent circular polarization performance and minimal polarization distortion. The antenna patterns (E-Plane and H-Plane) in Phase 4 are broader than in Phase 3, as displayed in Fig. 14. Although the gain slightly reduces to 6.5 dBi, the beam coverage improves, which is beneficial for wide-area communication applications.

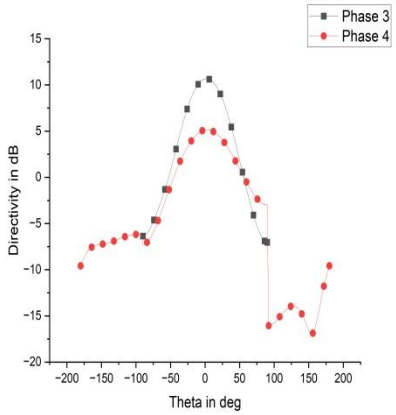

Fig. 12. Directivity plots of Phase 3 and 4 antennas

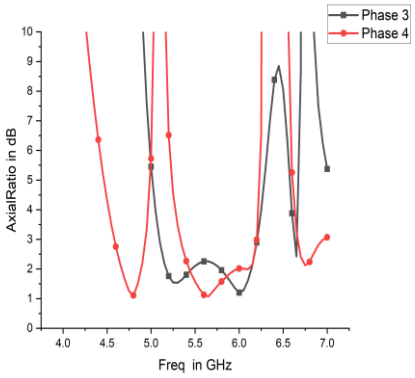

Fig. 13. Axial ratio plots of Phase 3 and 4 antennas

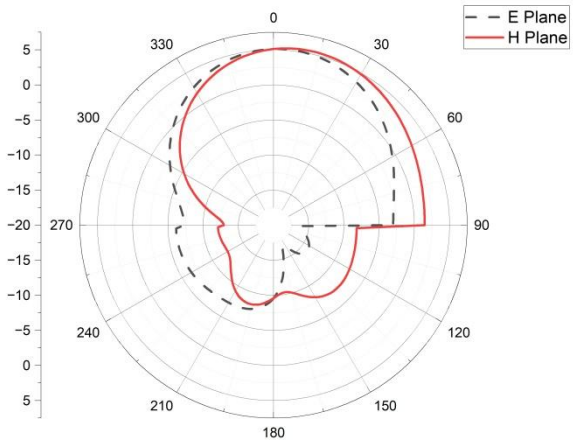

Fig. 14. Radiation pattern plot of Phase 4 antenna

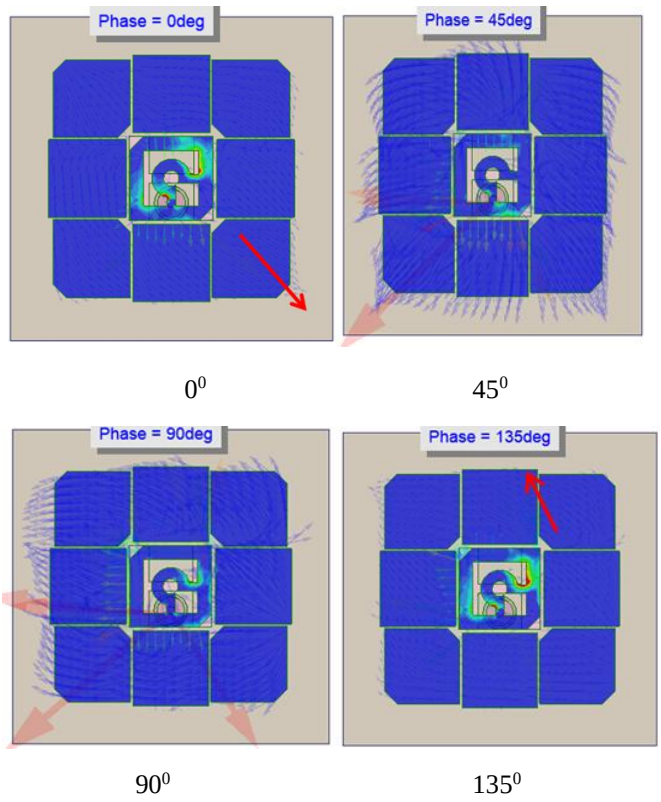

0^0 45^0

90^0 135^0

Fig. 15. Surface Current distribution at 4.95 GHz

The surface current distribution of the recommended antenna was analysed at various phase angles (0°, 45°, 90°, and 135°), as shown in Fig. 15. The results expose a clear clockwise rotation of the current on the radiating patch as the phase progresses. This rotating current pattern is a characteristic feature of RHCP behaviour.

The axial-ratio plots are demonstrated in Fig. 13. As seen, circular polarization (CP) occurs at 4.95 GHz, where the axial-ratio remains below 3 dB, confirming the presence of a CP mode at this frequency. Furthermore, two distinct CP bands can be observed at 4.8 GHz and 5.65 GHz, with each exhibiting an axial-ratio under 3 dB, which demonstrates efficient dual-band circular polarization across the operating frequency range.

Table II compares the four antenna phases (1–4). Impedance bandwidth improved from 0 GHz (Phase 1) to 2.12 GHz (Phase 4). Axial-ratio bandwidth also increased, enabling better circular polarization.

TABLE II
PERFORMANCE TABLE

Phase	Frequency (GHz)	Return Loss (dB)	Bandwidth (Hz)	Gain (dBi)	AR Bandwidth (Hz)
1	5.55	-4.52	0	6.8	-
2	5.25 & 7.45	-14.64 & -2.04	190 MHz (5.38-5.19) & 160 MHz(7.53 -7.37)	8 & 11.2	100 MHz(7.08 -6.98)
3	5.25 & 6.1	-25.89 & -9.10	1.12 GHz (6.24-5.12)	8.7 & 10.7	1.10 GHz(6.20-5.09)
4	4.95 & 5.40	-35.85 & -2.36	2.12 GHz (6.19-4.07)	5.4 & 6.5	360 MHz (4.94-4.58) & 870 MHz (6.20-5.33)

III. SIMULATED AND MEASURED RESULTS:

This section summarizes the performance evaluation of the suggested antenna designs at Phase 3 and Phase 4, along with the improvements achieved in some main parameters: return loss, bandwidth, gain, and circular polarization characteristics. The photographs of the fabricated antenna in front view and back view are shown in Fig. 16 and Fig. 17, respectively. Antenna performance was also measured using a Vector Network Analyzer (VNA) to validate S-parameters and return loss, as presented in Fig. 18.

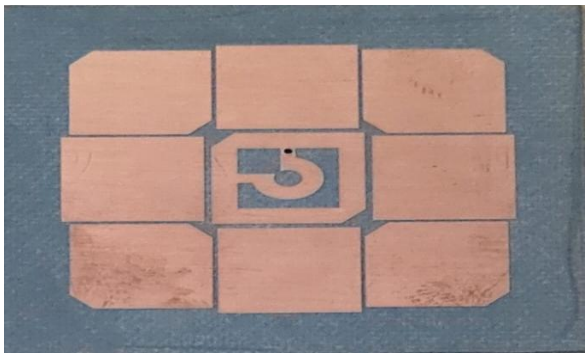

Fig.16. Photograph of Fabricated antenna (Front View)

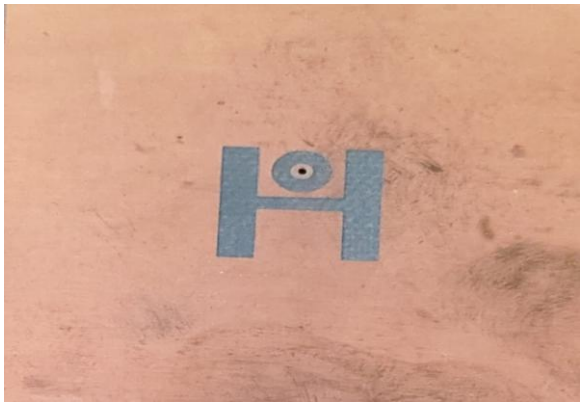

Fig.17. Photograph of Fabricated antenna (Back View)

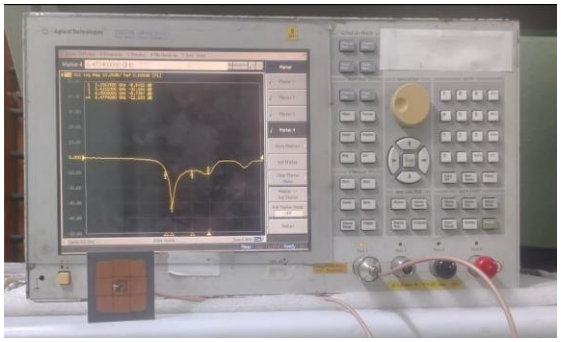

Fig.18. Photograph of Experimental setup using VNA

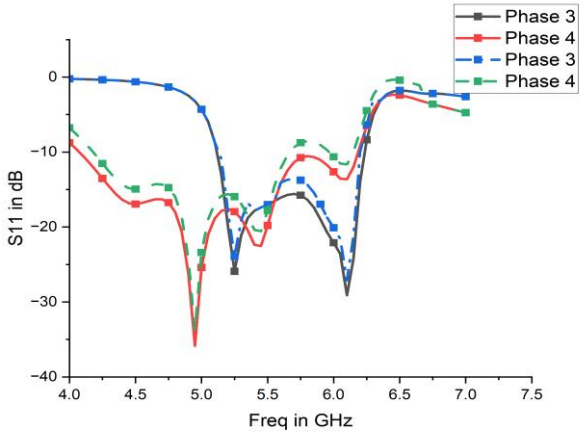

Fig. 19. Measured (Dotted lines) and simulated (Line) S-parameter plots of Phase 3 and 4 antennas.

The measured and simulated S-parameter results demonstrate good agreement for both Phase 3 and Phase 4 antennas, as depicted in Fig. 19. The reflection loss values closely follow the simulated curves, indicating that the designed antennas retain their impedance matching in practical implementation. Minor shifts in resonant frequencies between measured and simulated results may be due to fabrication tolerances and connector variations losses.

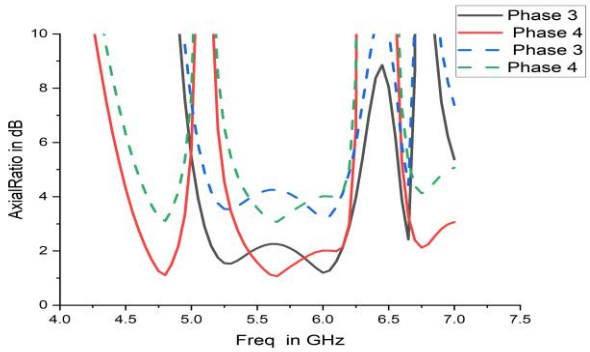

Fig. 20. Measured (Dotted lines) and simulated (Line) Axial ratio plots of Phase 3 and 4 antennas.

The axial-ratio plots for both phases show a close match between measured and simulated data, as depicted in Fig. 20. The 3-dB AR bandwidth observed in the measured plots confirms the antennas' circular polarization performance, with only minor deviations from the simulated results due to dielectric inconsistencies and alignment errors during measurement.

This plot clearly illustrates how the introduction of DGS in Phase 4 broadens the S-parameter curve. The dip in return loss around 4.95 GHz reaches nearly -36 dB, confirming excellent impedance matching. Phase 3 had a narrower bandwidth centred at 6.1 GHz.

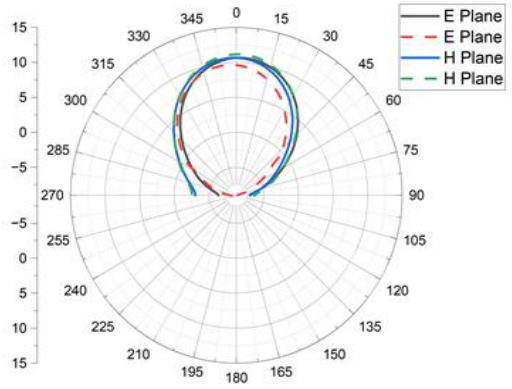

Fig. 21. Measured (Dotted lines) and simulated (Line) Radiation pattern plot of Phase 3 antenna

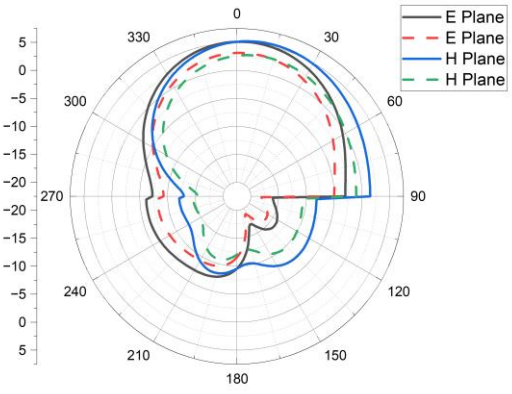

Fig. 22. Measured (Dotted lines) and simulated (Line) Radiation pattern plot of Phase 4 antenna.

The antenna patterns (E Plane & H Plane) for both Phase 3 and Phase 4 antennas display consistent behaviour between measured and simulated results, as displayed in Fig. 21 and Fig. 22. The main lobe direction and beam width are in good agreement, although small variations in side lobe levels and back radiation are observed. These differences may arise from environmental reflections and limitations of the measurement setup.

These figures collectively demonstrate that Phase 4, with DGS, provides better impedance bandwidth and polarization characteristics, whereas Phase 3 offers slightly superior gain. Depending on the application, either design could be advantageous.

TABLE III
COMPARISON OF ANTENNAS REPORTED IN LITERATURE

Antenna structure	Frequency range (GHz)	Return Loss (dB)	Impedance Bandwidth (%)	Axial Ratio (AR) Band-width (%)	Peak Gain (dBi)
[1]	6	>10	38	28.1	8.4
[3]	5.05 - 5.85	>10	14.7	16.6	9.1 - 10.8
[5]	2.33	>-10	6	6	11.0
[6]	7.1 - 10.2	>-10	36.2	33.6	10.0
[9]	2.25 - 3.0	>-10	38.2	28.6	8.4
[11]	5.01 - 5.87	>-10	15.9	11.8	12.5
[16]	3.46	>-10	6.4	6.4	7.7
[18]	5.05, 5.85	>-10	27	11	7.7
Proposed work	4.95 - 7.45	-35.85	48.8	22.2	11.2

The performance of various antenna designs across frequency range, return loss, impedance bandwidth, AR bandwidth, and peak gains, as shown in Table 3. The proposed antenna operates over a broad frequency range (4.95–7.45 GHz) and achieves a remarkably low reflection loss of -35.85 dB, indicating excellent impedance matching. It has the highest impedance bandwidth (48.8%), surpassing most existing designs, making it highly efficient for wideband applications. Although its AR bandwidth (22.2%) is lower than some wideband antennas like [6] (33.6%), it still ensures reliable circular polarization. With a high gain of 11.2 dBi, the proposed design competes with high-gain antennas such as [11] (12.5 dBi) and [5] (11.0 dBi), making it ideal for Wi-Fi, WiMAX, and X-band applications. Overall, this research offers a superior combination of bandwidth, gain, and polarization, making it a strong candidate for modern wireless systems.

IV. CONCLUSION

The development of this antenna design shows a systematic improvement in impedance matching, bandwidth, and circular polarization. The addition of parasitic patches enabled dual-band operation, while further optimisations enhanced bandwidth and axial ratio performance. The final integration of a Defective Ground Structure (DGS) permitted ultra-wideband operation, extending the bandwidth to over 2 GHz while preserving stable CP performance. With its high gain, wide bandwidth, and excellent polarization characteristics, this antenna is highly appropriate for modern wireless communication systems, including satellite communications and radar applications.

REFERENCES

[1] J Yang, W.W., Sun, W.J., Qin, W., Chen, J.X. and Zhou, J.Y., 2017. Broadband circularly polarised stacked patch antenna with integrated dual-feeding network. IET Microwaves, Antennas & Propagation, 11(12), pp.1791-1795.

[2] Yang, W., Zhou, J., Yu, Z. and Li, L., 2014. Single-fed low profile broadband circularly polarized stacked patch antenna. IEEE Transactions on Antennas and Propagation, 62(10), pp.5406-5410.

[3] Hussain, N., Tran, H.H. and Le, T.T., 2020. Single-layer wideband high-gain circularly polarized patch antenna with parasitic elements. AEU-International Journal of Electronics and Communications, 113, p.152992.

[4] Li, G. and Zhang, F.S., 2019. A compact broadband and wide beam circularly polarized antenna with shorted vertical plates. IEEE Access, 7, pp.90916-90921.

[5] Liu, Z.X., Zhu, L. and Zhang, X., 2019. A low-profile and high-gain CP patch antenna with improved AR bandwidth via perturbed ring resonator. IEEE Antennas and Wireless Propagation Letters, 18(2), pp.397-401.

[6] Oraizi, H. and Pazoki, R., 2012. Wideband circularly polarized aperture-fed rotated stacked patch antenna. IEEE Transactions on Antennas and Propagation, 61(3), pp.1048-1054.

[7] Weng, L.H., Guo, Y.C., Shi, X.W. and Chen, X.Q., 2008. An overview on defected ground structure. progress in electromagnetics research B, 7, pp.173-189.

[8] Noro, T. and Kazama, Y., 2005, July. A novel wideband circular polarization microstrip antenna-combination of different shaped antenna element. In 2005 IEEE Antennas and Propagation Society International Symposium (Vol. 3, pp. 467-470). IEEE.

[9] Baik, J.W., Lee, T.H., Pyo, S., Han, S.M., Jeong, J. and Kim, Y.S., 2010. Broadband circularly polarized crossed dipole with parasitic loop resonators and its arrays. IEEE Transactions on Antennas and Propagation, 59(1), pp.80-88.

[10] Deng, C., Li, Y., Zhang, Z. and Feng, Z., 2014. A wideband sequential-phase fed circularly polarized patch array. IEEE Transactions on Antennas and Propagation, 62(7), pp.3890-3893.

[11] Ding, K., Gao, C., Yu, T., Qu, D. and Zhang, B., 2016. Gain-improved broadband circularly polarized antenna array with parasitic patches. IEEE Antennas and Wireless Propagation Letters, 16, pp.1468-1471.

[12] Egashira, S. and Nishiyama, E., 1996. Stacked microstrip antenna with wide bandwidth and high gain. IEEE Transactions on Antennas and Propagation, 44(11), pp.1533-1534.

[13] Er-Rebyiy, R., Zbitou, J., Tajmouati, A., Latrach, M., Errkik, A. and El Abdellaoui, L., 2017, April. A new design of a miniature microstrip patch antenna using defected ground structure DGS. In 2017 International Conference on Wireless Technologies, Embedded and Intelligent Systems (WITS) (pp. 1-4). IEEE.

[14] Falade, O.P., Rehman, M.U., Gao, Y., Chen, X. and Parini, C.G., 2012. Single feed stacked patch circular polarized antenna for triple band GPS receivers. IEEE transactions on antennas and propagation, 60(10), pp.4479-4484.

[15] Khandelwal, M.K., Kanaujia, B.K. and Kumar, S., 2017. Defected ground structure: fundamentals, analysis, and applications in modern wireless trends. International Journal of antennas and Propagation, 2017(1), p.2018527.

[16] Li, Y., Zhang, Z. and Feng, Z., 2012. A sequential-phase feed using a circularly polarized shorted loop structure. IEEE Transactions on Antennas and Propagation, 61(3), pp.1443-1447.

[17] Pan, Y.M., Yang, W.J., Zheng, S.Y. and Hu, P.F., 2017. Design of wideband circularly polarized antenna using coupled rotated vertical metallic plates. IEEE Transactions on Antennas and Propagation, 66(1), pp.42-49.

[18] Shekhawat, S., Sekra, P., Bhatnagar, D., Saxena, V.K. and Saini, J.S., 2010. Stacked arrangement of rectangular microstrip patches for circularly polarized broadband performance. IEEE Antennas and Wireless Propagation Letters, 9, pp.910-913.

[19] Ta, S.X., Lee, K., Park, I. and Ziolkowski, R.W., 2016. Compact

crossed-dipole antennas loaded with near-field resonant parasitic elements. IEEE Transactions on Antennas and Propagation, 65(2), pp.482-488..

[20] Noro, T., Kazama, Y., Takahashi, M. and Ito, K., 2007, June. A study on the mechanism of wideband characteristics for single-fed stacked circularly polarization patch antenna. In 2007 IEEE Antennas and Propagation Society International Symposium (pp. 733-736). IEEE.

[21] Waterhouse, R.B., 1999. Design of probe-fed stacked patches. IEEE Transactions on Antennas and Propagation, 47(12), pp.1780-1784.

[22] Yang, W., Zhou, J., Yu, Z. and Li, L., 2014. Bandwidth-and gain-enhanced circularly polarized antenna array using sequential phase feed. IEEE Antennas and Wireless Propagation Letters, 13, pp.1215-1218.

[23] Wu, J., Yin, Y., Wang, Z. and Lian, R., 2014. Broadband circularly polarized patch antenna with parasitic strips. IEEE Antennas and Wireless Propagation Letters, 14, pp.559-562.

[24] Zhang, B., Zhang, Y.P., Titz, D., Ferrero, F. and Luxey, C., 2012. A circularly-polarized array antenna using linearly-polarized sub grid arrays for highly-integrated 60-GHz radio. IEEE Transactions on Antennas and Propagation, 61(1), pp.436-439.

[25] Nalanagula, R., Darimireddy, N.K., Kumari, R., Park, C.W. and Reddy, R.R., 2021. Circularly polarized hybrid dielectric resonator antennas: A brief review and perspective analysis. Sensors, 21(12), p.4100.

[26] Darimireddy, N.K., Reddy, R.R. and Prasad, A.M., 2020. Wideband circularly polarized cylindrical dielectric resonator antennas with rectangular curved slots [antenna applications corner]. IEEE Antennas and Propagation Magazine, 62(6), pp.65-73.